Production of oleogels from cellulose and starch cryogels: Morphological, thermal, mechanical, and viscoelastic properties

Laiane Carvalho [a,b], Igor Dal Osto Pereira [c], Larissa Andreani [b], Francisco Ricardo Cunha [c], Sandra M. Luz [d], Rafael Macedo Dias [a], Alysson M.A. Silva [e], Leonardo F. Valadares [b], Simone Monteiro [a,e,*] (iD)

[a] *Institute of Chemistry, University of Goiás, Goiânia, GO, Brazil*
[b] *Embrapa Agroenergia, Brasília, DF, Brazil*
[c] *Mechanical Engineering Department, Laboratory of Microhydrodynamics and Rheology, University of Brasília, DF, Brazil*
[d] *Automotive Engineering Department, Gama Campus, University of Brasília, DF, Brazil*
[e] *Mechanical Engineering Department, University of Brasília, Brasília, DF, Brazil*

ARTICLE INFO

ABSTRACT

Oleogelation offers a way to reduce trans fats and saturated fats in foods by structuring liquid oils. This study explores cryogels derived from cotton cellulose and potato starch as templates for soybean oleogel production. Cryogels were prepared using a freeze-drying method with cellulose and starch in various mass ratios (pure cellulose, pure starch, 20 cellulose/80 starch, 20 starch/80 cellulose, and 50 starch/50 cellulose) and then evaluated for mechanical and rheological properties. Composite cryogels provided enhanced mechanical strength, thermal stability, and oil retention, with pure cellulose cryogels achieving the highest oil absorption capacity (179.42 g/g). While adding starch reduced oil absorption, retention remained significant (18.95–55.59 g/g), with a 50/50 starch-cellulose blend exhibiting optimal oil retention (81.54 %). Rheological assessments showed shear-thinning behavior in all oleogels, with low-frequency dynamic tests revealing a solid-like, elastic response. The storage modulus (G′) increased with cellulose content, reaching 7×10^4 Pa, indicating robust elastic characteristics. The loss modulus (G″) results suggested larger fiber structures and increased collisional interactions with higher cellulose. These oleogels displayed a predominantly solid-like behavior at low frequencies, reflecting the effective structuring of oils through an oil sorption mechanism. This technique highlights cellulose-starch cryogels as viable oleogel templates for structuring edible oils.

1. Introduction

Oleogels have emerged as a promising alternative to trans and saturated fats, which are known to have adverse effects on human health (Puscas et al., 2020; Yang et al., 2024). These semisolid systems are formed by trapping liquid oil within a three-dimensional lattice without altering the oil's chemical properties (Manzocco et al., 2017; Patel et al., 2013). Beyond their applications in the food industry, oleogels are being explored in diverse fields, including drug delivery, cosmetic stability enhancement, environmental engineering, lubrication for mechanical engines, and materials science. (Patel et al., 2015; Wang et al., 2021).

Structuring agents or oleogelators, such as wax, lecithin, esters, ceramides (low molecular weight), and proteins or polysaccharides (high molecular weight), are commonly used for oleogation (Li et al.,

2022). High molecular weight biopolymers, like polysaccharides, are advantageous due to their effectiveness at lower concentrations and their established use as structuring, stabilizing, or thickening agents in water-based food systems. Additionally, oleogels made with these polymers exhibit viscoelastic properties influenced by molecular weight, conformation, and concentration. Their GRAS (Generally Recognized As Safe) status and consumer acceptance as food additives further support their suitability for structuring edible oils (Davidovich-Pinhas, 2019; Patel, 2018).

Oleogelation can occur through direct or indirect structuring methods. The direct method involves dispersing a structuring agent directly into the oil phase, typically at high temperatures (above the gelator's melting point) with mechanical stirring. However, this approach can degrade nutraceutical compounds and promote oil

---

oxidation. (Barroso et al., 2024; Kavya et al., 2022; Liu et al., 2023). Therefore, indirect approaches have been proposed, such as emulsion template, solvent exchange, and porous solid materials, such as foam and aerogels/cryogels (Kavya et al., 2022). Patel et al. (2013) proposed an alternative oil structuring method using hydroxypropyl methylcellulose (HPMC). By foaming and lyophilizing the HPMC solution, they created a porous structure with a high oil absorption capacity, resulting in oleogels exhibiting solid-like rheological properties under shear. However, cellulose derivatives like HPMC are costly, highlighting the need for more affordable alternatives (Ghahremani et al., 2024).

Porous structures like cryogels or aerogels are essential for trapping oil within a semisolid matrix to produce oleogels. These materials, known for their high surface area, porosity, and low density, are widely studied for sorption processes. They are typically derived from dispersions or gels and dried using supercritical CO_2 or freeze-drying methods (Abdullah et al., 2022; Lavoine & Bergström, 2017). The cryogel/aerogel-templated method is straightforward, requiring only oil absorption into the porous matrix. This approach offers enhanced protection for temperature-sensitive nutrients and improved antioxidant capacity compared to direct oleogelator dispersion in oil (Zhao et al., 2023). Moreover, bio-based cryogels/aerogels made from biopolymers are safe, biocompatible, and biodegradable.

Starch, an edible polysaccharide with low toxicity and non-allergenic properties, forms gels when heated in an aqueous medium, making it a versatile material (Zhu, 2019). However, porous starch-based materials face limitations due to their hydrophilicity and low mechanical strength. To overcome these challenges, incorporating another component into the material's solid structure can enhance its properties (Ago et al., 2016).

Recent studies have explored the development of hybrid and composite aerogels and cryogels for diverse applications. Alavi and Ciftci (2023) reported that starch aerogels enhanced with chitosan exhibited significantly reduced shrinkage and superior oil structuring capabilities compared to pure starch aerogels, attributed to improved macroporosity employed a dual-reinforcement strategy combining sodium carboxymethylcellulose and soy protein isolate with electrostatic adsorption and citric acid crosslinking to produce aerogel-templated oleogels. This approach significantly enhanced the mechanical properties, elasticity, and oil-holding capacity of the oleogels. Similarly, Jiang et al. (2022) prepared hydroxypropyl-methylcellulose cryogel templates reinforced with flaxseed gum for oleogel formation. They observed that flaxseed gum and guar gum cryogels facilitated faster oil absorption due to larger pores. In contrast, κ-carrageenan and linseed gum cryogels, with smaller pores and greater rigidity, demonstrated higher elastic moduli and oil retention. In contrast, softer cryogels made from gum Arabic were more deformable under external forces, reducing their oil retention capacity.

Combining starch with biopolymers such as agar or microcrystalline cellulose has proven effective in modulating aerogel properties (Dogenski et al., 2020). Over the past decade, research has shown that blending cellulose and starch enhances composites' mechanical properties, moisture resistance, and thermal stability (Ahmad et al., 2022; Yildirim et al., 2014; Zhao et al., 2021). For instance, Zhao et al. (2021) demonstrated that incorporating cellulose nanofibers into starch/clay aerogels improved structural stability during freezing and freeze-drying, enhanced compressive strength, increased moisture resistance, and improved shape recovery and thermal stability. Despite these promising outcomes, studies on hybrid/composite aerogels or cryogels incorporating cellulose and starch remain limited, particularly for edible oleogelation. Therefore, this study focuses on developing edible composite cryogels using cellulose and starch.

Cellulose, an abundant biopolymer, constitutes a significant fraction of dried biomass from plants and is also found in some animals and microorganisms. It is commonly sourced from materials such as straw, cotton, wood, and bagasse (Gu et al., 2022). Microfibrillated cellulose (MFC), characterized by its web-like structure, fiber diameters of 20–60 nm, and lengths of several micrometers, is produced through homogenization processes. Due to its reinforcing properties and strong entangled nanoporous network, MFC is widely used in nanocomposites (Lavoine et al., 2012; Siqueira et al., 2010). Additionally, fibrillated cellulose exhibits enhanced rheological characteristics and serves as a non-caloric stabilizer, gelling agent, thickener, and flavor carrier in food at low concentrations (Wüstenberg, 2014). Its dietary fiber content also provides health benefits, such as preventing and managing gastrointestinal disorders (Gill et al., 2021; Ong et al., 2020).

While incorporating cellulose into starch-based cryogels offers advantages, its application in food-grade oleogel production remains unexplored. Alavi and Ciftci (2023) recently studied the rheological properties of oleogels composed of soybean oil mixed with corn starch, either neat or combined with chitosan at various ratios, highlighting the potential for further innovations in this field.

In this context, this study aimed to investigate the effect of the combination of starch and cellulose on the physicochemical properties and functionality of cryogels intended for food-grade oleogel production.

2. Materials and methods

2.1. Materials

Commercial hydrophilic cotton and soybean oil were purchased in a local market in Brasília, Brazil. Potato starch (product reference: S2004) was purchased from Sigma Aldrich (USA). Distilled water was used to prepare hydrocolloids.

2.2. Preparation of cryogels

The aqueous cellulose suspension was prepared following Cheng et al. (2017). Cotton fibers were cut into 1 cm squares and dispersed in water (0.25 g cotton/100 g water) using a kitchen blender with a filter (Britannia BLQ1280, 1150 W, Brazil). Shearing was performed with a disperser (UltraTurrax T25 D S32, IKA, Germany) for 10 cycles (5 min each) at 18,000 rpm. Gelatinized starch was prepared following Teles dos Santos et al. (2013) by dispersing soluble potato starch (4 g starch/100 g water) in distilled water, mixing with a spatula, and heating at 70 °C with constant stirring for 30 min. The solution was cooled to room temperature. The final solids content was determined by drying 20–25 g of the samples at 105 °C for 24 h (Yildirim et al., 2014). Cryogel's production was adapted from the literature. Composite cryogels were prepared by mixing starch (S) and cellulose (C) dispersions in varying weight ratios: S0C100, S20C80, S50C50, S80C20, and S100C0. The mixtures were homogenized using a high-shear disperser (Ultra-Turrax, IKA, USA) at 10,000 rpm for 1 min, poured into molds, and frozen at −18 °C for 24 h, followed by 4 h at −80 °C. Finally, the materials were freeze-dried (Liotop K120, Brazil) at −98 °C and 40 kPa for 96 h to obtain the monolith cryogels.

2.3. Volumetric shrinkage

The volumetric shrinkage (V_S) of the cryogels, expressed in percentage, was determined in triplicate by measuring the volume change during freeze-drying (Equation (1)). The volumes (cm^3) of the aqueous dispersion (V_d) and the cryogel (V) were calculated using diameter and height measurements taken before and after freeze-drying.

$$Vs = \frac{V_d - V}{V_d} \times 100 \ (\%). \tag{1}$$

2.4. Density and porosity

The bulk density (ρ_0) of the cryogel monoliths, expressed in g·cm^{-3}, was determined in triplicate (Equation (2)). Porosity (ε), expressed in percentage, was calculated from ρ_0 and ρ according to Equation (3):

$$\rho_0 = \frac{m}{V}. \tag{2}$$

$$\varepsilon = \left(1 - \frac{\rho_0}{\rho}\right) \times 100 \ (\%), \tag{3}$$

Where m is mass, V is volume (cm^3), ρ_0 and ρ are the experimental cryogel's and the biopolymers' theoretical density (g·cm^{-3}). The theoretical density was calculated using a weight-average approach (Equation (4)) (Paulauskiene et al., 2022):

$$\rho = 1 / (\phi_c + \phi_s), \tag{4}$$

where $\phi_c = w_c/\rho_c$ and $\phi_s = w_s/\rho_s$. Subscripts c and s denote cellulose and starch, respectively, with w representing the mass fraction (dimensionless) and ρ the density (g·cm^{-3}). The densities used were 1.50 g·cm^{-3} for cellulose (cotton fiber) and 1.45 g·cm^{-3} and the subscripts c denotes cellulose and s starch, respectively (Paulauskiene et al., 2022).

2.5. Specific surface area

The surface area of the cryogels was measured via N₂ adsorption/desorption (Autosorb iQ Station 2, Quantachrome Instruments, Germany). Cryogels were molded to fit into 9 mm glass tubes, and samples (0.003–0.05 g) were degassed at 120 °C for 24 h before analysis.

2.6. Micromorphology and crystallinity

The surface morphology of the cryogels was analyzed using Scanning Electron Microscopy (SEM) with 1 nm resolution.

(Sigma-HV, Zeiss, UK). Samples were fragmented with a spatula, fixed onto stubs with carbon tape, and coated with a gold layer via sputtering (QT150T-ES, Quorum Technologies, UK). The crystal structure was determined by X-ray diffraction (XRD) (Lab XRD-6000, Shimadzu, Japan), with scattered radiation measured in the 2θ range of 4°–30° at a scanning speed of 2°/min and increments of 0.02°.

2.7. Fourier Transform Infrared Spectroscopy (FTIR)

The pure and composite cryogels were analyzed using Fourier Transform Infrared Spectroscopy (FTIR) (Affinity-1, Shimadzu, Japan). Dried samples (60 °C, 24 h) were mixed with ~200 mg of KBr and pressed into pellets. Infrared spectra were recorded in the wavenumber range of 400–4000 cm^{-1} with a resolution of 4 cm^{-1} and 32 scans at room temperature.

2.8. Thermogravimetric analysis

Thermogravimetric analysis (TGA) and differential scanning calorimetry (DSC) were simultaneously performed using an SDT Q600 (TA Instruments, USA). Samples were heated in alumina pans from 25 °C to 600 °C at a rate of 10 °C·min^{-1} under a nitrogen flow of 100 mL min^{-1}.

2.9. Mechanical compression test

Cryogel and oleogel samples were tested using a universal testing machine under ambient conditions (23 °C, 60–70% humidity). Samples, prepared according to ASTM standards, were compressed to 60% deformation. Stress-strain curves were used to determine the modulus of elasticity, yield strength, and compressive strength. Hardness was measured as the maximum force required for 30% deformation. Results, expressed as means ± root mean square (RMS), were based on at least three measurements and analyzed using one-way ANOVA, Tukey's test, and T-tests at a 5% significance level (Abdollahi et al., 2019; Li & Zhang, 2023).

2.10. Oil absorption and holding capacity

The oil absorption capacity (C$_{oa}$) of cryogels, expressed in percentage, was measured in triplicate using the ratio of absorbed oil mass to the cryogel's initial mass. Cryogels (M_0) were immersed in soybean oil for 5 min, drained for 30 s to remove excess oil, and re-weighed (M). Oil holding capacity (C$_{oh}$), expressed in percentage, was determined following Manzocco et al. (2017), where oleogel samples were centrifuged at 10,000 g for 20 min in a 15 mL tube containing absorbent paper. Calculations used Equations (5) and (6):

$$C_{oa} = \frac{(M - M_0)}{M_0}. \tag{5}$$

$$C_{oh} = \frac{m_0}{m_1} \text{ x } 100 \ (\%), \tag{6}$$

Where m_0 and m_1 represent the oil weight (g) in the cryogel after and before centrifugation. Data were analyzed using one-way ANOVA followed by Tukey's test at a 5% significance level. Group comparisons were further evaluated using the T-test at a 5% significance level.

2.11. Rheological characterization in steady and unsteady shear flows

To evaluate the viscoelastic response of the oleogels examined here, the Rheological measurements were performed on a torque-controlled MCR 301 (Anton Paar, Austria). The gap was small (typically 0.4 mm) and must be filled to obtain representative measurements. In steady shear measurements, the stress σ_R (N/m^2) is computed by the rheometer using the following Equation (7) (Bird et al., 1987):

$$\sigma_R = \frac{T_0}{2\pi R^3}\left[3 + \frac{d \ln (T_0)}{d \ln (\dot{\gamma}_R)}\right], \tag{7}$$

where T_0 (N/m) is the applied torque, R (m) is the disk radius, and $\dot{\gamma}_R$ (1/s) the applied shear rate at the rim of the disk.

The small amplitude oscillatory shear (SAOS) experiments were carried out to determine the dynamic response of the oleogel in terms of an elastic modulus $G'(\omega)$ (N/m^2) and the viscous modulus $G''(\omega)$ (N/m^2). Specifically, for rheometers of parallel-disk, the viscoelastic material functions can be obtained experimentally by using (Cwalina & Wagner, 2016; Pereira & Cunha, 2023):

$$G'(\omega) = \frac{2hT_0 \cos (\beta_0)}{\pi R^4 \theta_0} \text{ and } G''^{(\omega)} = \frac{2hT_0 \sin(\beta_0)}{\pi R^4 \theta_0}, \tag{8}$$

where h (m) is the height of the gap between the disk, β_0 (dimensionless) is the phase angle, and θ_0 (dimensionless) denotes the angular displacement.

The first experiment performed was a permanent isothermal simple shearing flow. The procedure involved placing a small amount of the fluid (less than 1 ml) in the rheometer test section, followed by applying a shear rate $\dot{\gamma}$ ranging from 1 to 500 s^{-1}. The data was collected at a frequency of 5 points per decade.

The second experimental approach involved SAOS. The experiments were carried out with a sufficiently small angular deformation so that G$'$ must be independent of γ and dependent on the forcing frequency. A sweep strain γ$_0$ = 0.1% was verified for all oleogels examined and is characterized by a linear viscoelastic response (LVR). The end of the LVR was identified by finding the sweep strain at which the initial value of G' changes by 1%. Therefore all experiments in SAOS were carried out for the strain less than or equal to the sweep strain. Under this condition, the viscoelastic moduli are approximately constant at low frequency. In addition, oleogel microstructures were performed by digital images analysis using a standard optical microscope Olympus BX51 with 50× of magnification and a digital camera UC30. The captured micrographs enable the investigation of microstructure details, including anisotropy and the distribution of small-scale constituents within the complex fluid.

3. Results and discussion

3.1. Characterization of the precursor solutions and cryogels

Characterizing the precursor solutions and cryogels is essential to understanding their properties and potential applications. Table 1 presents the bulk density, porosity, and cryogels ranged from 0.003 to 0.056 g cm^{-3}, and the porosity varied from 96.2% to 99.8%. As expected, lower solids content led to a less dense and more porous structure. This inverse relationship between solids content and porosity can be attributed to the increased bonding between starch and cellulose, which fills the same volume (Yildirim et al., 2014).

In the production of cryogels, it is also common to observe a decrease in volume after freeze-drying due to the solvent removal (water), the composition, and the degree of gelling of the precursor material (Druel et al., 2017; Mehling et al., 2009). Regarding the volumetric shrinkage of cryogels produced, values were relatively close, ranging from 30.5% to 33.0%, with no statistical difference between the materials.

Concerning the specific surface area values of pure and composite cryogels, the values ranged from 6.9 (pure starch) to 52.4 m^2/g (pure cellulose), and these values were consistent with those reported in the literature for cryogels (7.7–66 m^2/g) (Baudron et al., 2019; Pääkkö et al., 2008; Sehaqui et al., 2010). The specific surface areas of the cryogels produced were inversely proportional to the solids content: an increase in the concentration of the precursor solution resulted in an increase in density with a less porous structure and, therefore, a smaller surface area. Other studies have already demonstrated this inverse relationship (Ciftci et al., 2017; Pääkkö et al., 2008; Sehaqui et al.,

Table 1
Textural and mechanical properties of cryogels and oleogels.

Sample	S0C100	S20C80	S50C50	S80C20	S100C0
Cryogel					
Solid-water content (%)	0.25	1.00	2.13	3.25	4.00
ρ_0 (g·cm^{-3})	0.003 ± 0.000[a]	0.013 ± 0.000[b]	0.030 ± 0.001[c]	0.047 ± 0.000[d]	0.056 ± 0.002[e]
ε (%)	99.892 ± 0.048[a]	99.167 ± 0.071[b]	98.027 ± 0.068[c]	97.081 ± 0.046[d]	96.201 ± 0.127[e]
V_S (%)	30.5 ± 0.5[a]	31.2 ± 1.5[a]	33.1 ± 1.5[a]	33,7 ± 0.4[a]	33.0 ± 1.9[a]
S_a [BET] (m^2/g)	52.4	–	26.6	–	6.8
Compressive strength (kPa)†	0.70 ± 0.0[a]	4.22 ± 0.92[a]	28.13 ± 1.75[b]	50.66 ± 2.14[c]	56.83 ± 3.50[d]
Elastic modulus (kPa)	0.01 ± 0.00[a]	0.11 ± 0.03[a]	1.39 ± 0.18[b]	2.40 ± 0.34[c]	1.05 ± 0.22[b]
Yield strength (kPa)	0.46 ± 0.10[a]	1.38 ± 0.31[a]	7.82 ± 1.06[b]	11.11 ± 1.14[c]	9.29 ± 1.46[b]
Hardness (N)	0.14 ± 0.06[c]	1.00 ± 0.21[bc]	6.58 ± 0.28[b]	10.68 ± 1.47[a]	8.70 ± 0.91[a]
Oil Absorption Capacity (g/g)	179.42 ± 2.59[a]	55.59 ± 1.76[b]	29.74 ± 1.30[c]	18.95 ± 0.66[d]	14.76 ± 0.62[e]
Oil Holding Capacity (%)	56.55 ± 4.59[d]	66.78 ± 5.36[b]	81.54 ± 1.29[a]	74.94 ± 2.36[ab]	79.55 ± 2.05[a]
Oleogels					
Compressive strength (kPa)‡	–	3.69 ± 0.85	17.87 ± 0.80	45.03 ± 11.55	55.82 ± 10.26
Elastic modulus (kPa)	–	0.11 ± 0.04	0.59 ± 0.14	3.10 ± 1.06	2.03 ± 0.77
Yield strength (kPa)	–	1.20 ± 0.21	7.96 ± 2.00	16.32 ± 3.63	15.76 ± 3.16
Hardness (N)	0.22 ± 0.08[d]	0.96 ± 0.34[c]	5.00 ± 0.46[b]	13.28 ± 4.63[a]	15.28 ± 2.98[a]

ρ_0 = bulk density, ε = porosity, V_S = volumetric shrinkage and S_a = specific surface area. Results are expressed as mean values ± standard deviation of three replicates. Different superscript letters within the same lign represent significant differences (p < 0.05). † 60 % deformation; ‡ 50 % deformation, higher deformation values led to oil loss.
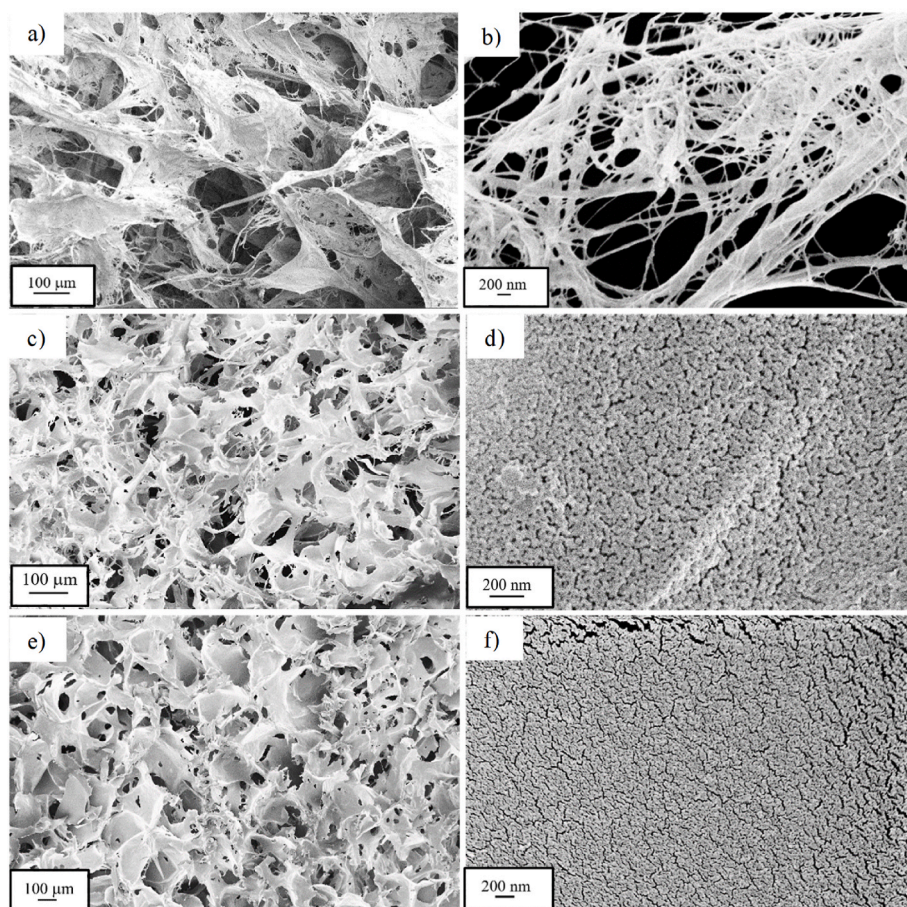
2011).

3.1.1. Cryogels microstructure analysis

The surface morphology of cryogels was examined using SEM images, revealing distinct differences in their microstructures. These differences are attributed to the precursor gel and the formation of ice crystals during freezing and drying (Abdullah et al., 2022). Ice crystals compress the gel network, and their sublimation leaves air spaces that form the material's pores. In pure cellulose cryogels (Fig. 1a), a three-dimensional network of web-like structures is observed, resulting from capillary forces and hydrogen bonds during the freeze-drying process (Chen et al., 2011). Fig. 1b shows the cellulose cryogel's macroporous structure, with internal micro/mesopores formed by fibrils of varying diameters.

In samples with equal concentrations of starch and cellulose (Fig. 1c), conglutinated structures featuring fibrils embedded in the starch matrix were observed, similar to the findings of Yildirim et al. (2014). The cellulose fibers were coated here, protecting them from capillary forces during freezing and drying. In contrast, pure starch cryogels (Fig. 1d) displayed more compact and dense structures in sheets or plates. These leaf-like structures are typically attributed to the slow growth of water crystals, which compress the gel lattice into planar aggregates (Baudron et al., 2019). Additionally, according to Chen et al. (2014), the microstructure of cryogels is influenced by gel viscosity, with less viscous gels offering less resistance to ice crystal formation, leading to the development of lamellar ice layers.

In addition, at higher magnification (Fig. 1d and f), some visible cracks are observed in the starch-containing cryogels, probably formed to relieve the tension induced by shrinkage during freeze-drying (Kenar et al., 2014). In addition, these fissures have widths of a few nanometers and, therefore, also represent a mesoporous microstructure (*i.e.*, pores with diameters between 2 and 50 nm) in these cryogels.

3.1.2. Crystallinity and composition of cryogels

The crystallinity of the cryogels was investigated using XRD (Fig. 2a). The diffractogram of sample S100C0 shows peaks in approximately 2θ = 22° and 17°, corresponding to the starch crystalline phase. The pure celulose, sample S0C100, exhibits a doublet in 2θ = 14.8° and 16.5° and a main peak at 2θ = 22.8°, indicating the crystallinity of cellulose type I and confirmed in the studies of Aguayo et al. (2018) and Park et al. (2010). The decrease of the concentration of the cellulose and, consequently, the increase of the concentration of starch in the samples S20C80, S50C50 and S80C20 promote a rise in the FWHM of the main peaks, indicating a reduction of crystallinity and suggesting that starch recrystallization occurs during the cooling of the aqueous solution in sample preparation (Ratnayake & Jackson, 2007; Wang, Peng, et al., 2015). This XRD pattern is characteristic of B-type starch, commonly found in tuber starches. Consequently, the starch presence, in addition to diluting cellulose, as reported in the literature (Ek et al., 2021), also reduce the overall degree of crystallinity in the system, which further impacts the structural properties of the cryogels.

The micromorphology and crystallinity of cryogels can greatly influence the macrophysical properties of the material. A denser and microporous structure can result in better compressive properties, mainly due to the strong intermolecular bond (Wang et al., 2021). Besides, materials with high porosity are generally more desirable for the effective immobilization of active substances, oils, and drugs, which can be useful in a variety of applications involving oil absorption, controlled release, and nutritional delivery (Chen & Zhang, 2020; Li et al., 2022). Thus, the structural arrangement capable of trapping and retaining oil depends on a balance between density and porosity, so the cryogel must be porous to absorb a large amount of oil and sufficiently dense and cohesive to retain it. Crystallinity affects mechanical properties such as the strength and stiffness of cellulose and cellulose-derived materials. Higher cellulose crystallinity increases Young's modulus, density, and hardness (Rongpipi et al., 2019). Higher starch crystallinity produces

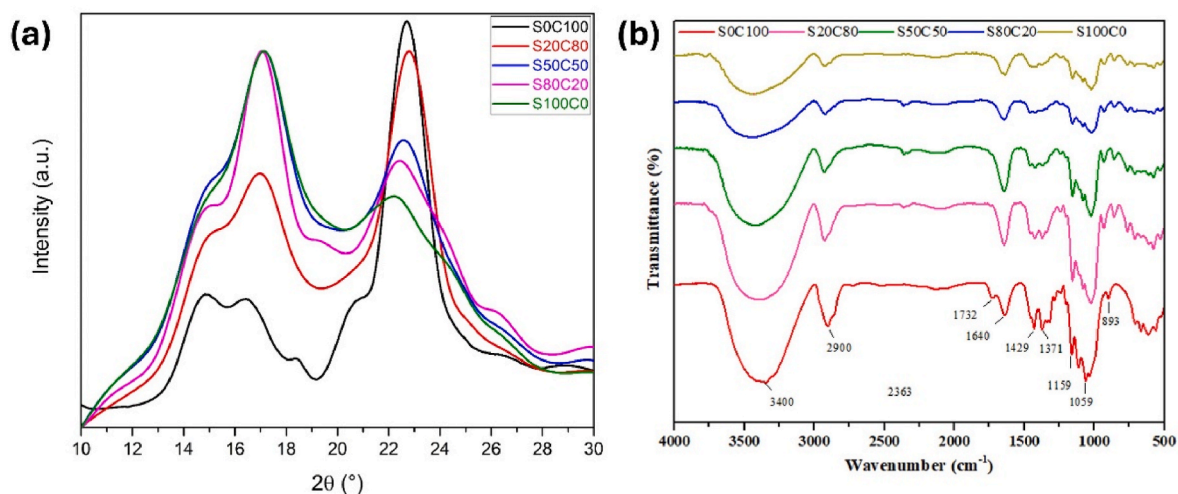**Fig. 1.** SEM images of the cryogels: S0C100 (a,b) S50C50 (c,d) S100C0 (e,f).

Fig. 2. a) X-ray diffraction and b) FTIR Spectra of cryogels.

stronger and more brittle starch gels and the corresponding cryogels (Zou & Budtova, 2020). The higher thermal resistance associated with cellulose is mainly related to the intra and inter-molecular hydrogen bonds (Poletto et al., 2014).

A more in-depth structural analysis of the aerogels obtained was performed using the FTIR technique, and the chemical bonds of the materials were characterized. The spectra of the aerogels studied are presented in Fig. 2b, and the signals observed were compared to the spectra of cellulose and starch reported in the literature, demonstrating

no chemical reactions between biopolymers. A detailed analysis of FTIR spectra is available in the Supplementary Material.

3.2. Thermal analysis of cryogels

The thermal stability of the cryogels was investigated through the thermogravimetric technique. The thermogravimetric curves (TGA and DTG) and DSC of the samples of pure microfibrillated cellulose, pure starch, and cellulose/starch composites are shown in Fig. 3. Table S1
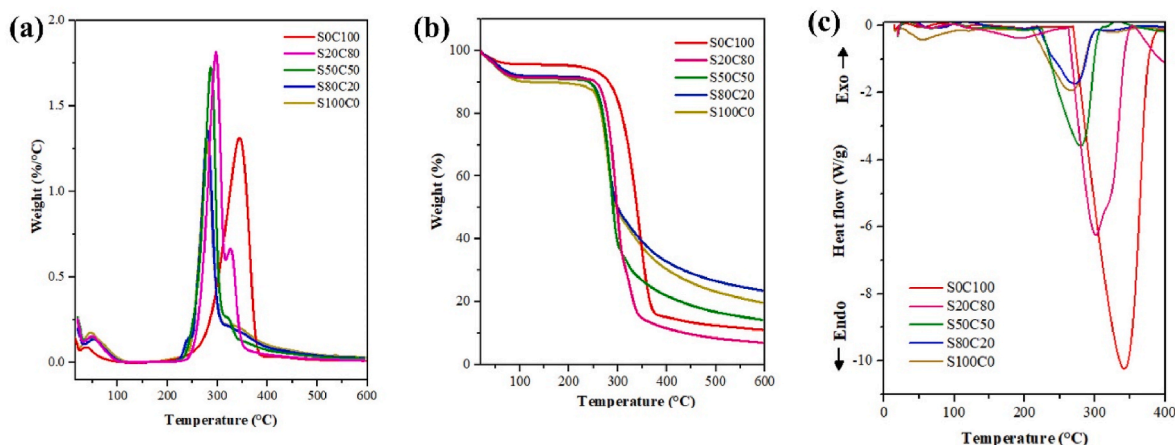
Fig. 3. Thermogravimetric analyses of pure cellulose (S0C100), pure starch (S100C0), and composite cryogels (S20C80, S50C50, and S80C20) cryogels. (a) TGA curves, (b) DTG curves, and (c) DSC curves.

shows the details of these curves and presents the thermal events for pure and composite cryogels.

Starch cryogels and their composites exhibited higher water loss at the process's initial stages than the pure cellulose cryogel (Fig. 3a). This outcome aligns with expectations, considering the inherently hydrophilic nature of starch (Hassan et al., 2020). The onset temperature of all cryogels was lower than that of pure cellulose cryogel, indicating that adding starch reduces thermal stability. Nevertheless, during the heating of the samples from 20 to 600 °C under a nitrogen atmosphere, S0C100 and S100C0 exhibited residual weights of 11.09% and 19.68%, respectively. This difference can be attributed to the increase in cellulose's superficial area due to the microfibrillation process and porous structure of cryogel enlarging the mass loss (Teles et al., 2021). Particularly, the residue of S80C20 surpassed that of all other cryogels, signifying that this blend of cellulose and starch offered enhanced thermal stability. This observation can be attributed to the improved structural and spatial arrangement facilitated by the interaction between fibers and starch in this specific composition.

Four weight loss stages were identified in the DTG curves (Fig. 3b), with peaks of varying intensities among the cryogels. The first stage occurs at low temperatures (less than 100 °C) and is attributed to the evaporation of water adsorbed on the material. The second stage appeared as shoulder and was identified only in the samples with the highest starch contents (S80C20 and S100C0) in the 230–250 °C range, indicating starch degradation (Teles et al., 2021). The third stage of mass loss can be clearly observed in the DTG curves in the range of 250–310 °C, which is due to starch degradation and burning, and in the range of 250–390 °C due to cellulose degradation. The final weight loss occurs in the fourth stage as a shoulder (315 °C–350 °C), which is associated with the thermal degradation of the cellulose in the composite. This way, as cellulose is added to the composites, their thermal stability improves significantly. In addition to the fact that cellulose is semicrystalline, this greater resistance to degradation can be attributed to the interactions between starch and cellulose, resulting in a decrease in the mobility of macromolecules (Spiridon et al., 2013). Therefore, the addition of cellulose microfibers into the starch matrix resulted in a compact structure, improving the thermal stability of the cryogels, which encouraged the industrial applications of these materials, especially for the preparation of oleogels, which require enhanced thermal stabilities either to favor the storage and the processing of food (Ahmad et al., 2022; Li et al., 2023).

3.3. Mechanical properties

In developing new materials, mechanical properties like stress strength and hardness are crucial for evaluating potential applications.

Table 1 illustrates the mechanical properties of the studied cryogels. The stress-strain curves (Table 1) display a typical behavior for porous materials, featuring three distinct regions commonly found in biopolymer-based cryogels/aerogels: elastic, plastic, and densification regions (Wang et al., 2018). An elastic region is initially observed, followed by an extensive plateau stage, where the stress increases weakly with increasing tension, and the material begins to deform irreversibly. Then, an abrupt increase in stress occurs at about 50–60% deformation, suggesting a complete fracture of the structure and the beginning of densification (Arboleda et al., 2013).

The increase in the solids content and, therefore, in the density of the cryogels correlated with the modulus of elasticity and tensile strength. Nonetheless, the pure starch cryogel (S100C0) exhibited poor mechanical properties. The addition of microfibrillated cellulose (MFC) produced better flexural properties, acting as a reinforcement to the starch cryogel. This finding was probably due to good dispersion and the micro size of cellulose that allowed an effective contact area with the starch matrix. Furthermore, the chemical similarities between starch and cellulose may induce a strong intermolecular interaction between the molecules through hydrogen bonding (Nordin et al., 2018).

Compressive strength increased with density and starch content, with pure cellulose cryogel being the least resistant due to its lower solids content. The S80C20 cryogel showed the highest elastic modulus and yield stress, indicating superior elasticity. In contrast, the S50C50 cryogel exhibited more plasticity, with an extended plateau region. These results suggest starch enhances elasticity, while small amounts of cellulose add plasticity and reinforcement, improving flexibility and elasticity (Ago et al., 2016; Sehaqui et al., 2011). The higher density of starch cryogels combined with cellulose fibers creates effective physical entanglement, enhancing mechanical properties. Compared to starch cryogels at higher concentrations (10%–15%), which broke at ~30% deformation, lower starch concentrations favor cryogel formation. Additionally, microfibrillated cellulose offers better flexibility than microcrystalline cellulose, primarily increasing stiffness (Dogenski et al., 2020).

3.4. Oleogel characterizations

3.4.1. Oil absorption, oil holding capacity and hardness

The cryogel produced was tested for its ability to trap an oil-liquid phase and hold this liquid phase in its structure. Fig. 4 presents digital photographs of the aerogels and oleogels evaluated in this study. The results of these tests, oil absorption and holding capacity, are shown in Table 1. Starch reduced the oil absorption capacity, with pure cellulose cryogel (S0C100) achieving the highest value at 179.42 g/g and pure starch cryogel (S100C0) the lowest at 14.76 g/g. Oil absorption
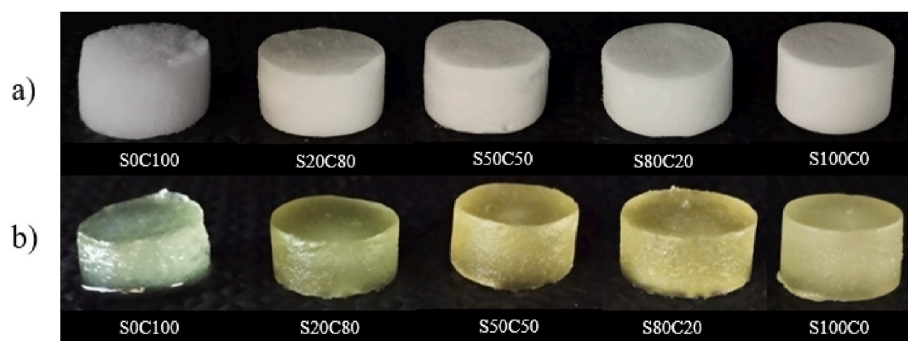
Fig. 4. Digital photographs of the cryogels (a) and oleogels (b) evaluated in this study.

capacities exceeding 160 g/g have been reported for cellulose-based materials, with values reaching up to 288 g/g (He et al., 2021; Wang, Peng, et al., 2015). This difference arises from the amphiphilic nature of cellulose, which enhances oil-trapping, and the polymer network's organization and internal architecture (Manzocco et al., 2017). According to "Lindman's hypothesis," water binds to OH groups aligned with the cellulose chain plane, while nonpolar compounds bind to C–H groups in lipophilic regions (Glasser et al., 2012). Higher starch concentrations increased density, reducing pore formation and oil-trapping ability.

Adding starch significantly enhanced the oil holding capacity, with cryogels containing higher starch content showing the greatest oil retention. Conversely, the S0C100 oleogel exhibited very poor oil-holding capacity. This outcome can be attributed to the weak network strength of the S0C100 cryogel, characterized by its low hardness. Consequently, the oleogel's network structure was more susceptible to collapse under external forces, leading to significant oil leakage (Jiang et al., 2022).

The combination of starch and cellulose fibers seems to achieve an optimal structural arrangement at S50C50, which exhibited a high oil retention capacity (81.54%). This enhanced retention may be attributed to the cryogel's greater plasticity, as observed in its stress vs. strain curve. Plastic materials can redistribute internal porosity during deformation, creating pathways and spaces that allow oil to penetrate and be retained more effectively. This behavior supports efficient oil retention under varying conditions. Comparable results have been reported for soybean oleogels structured with monopalmitate and carnauba wax (Yang et al., 2020).

The mechanical properties of the oleogels were assessed using compression test curves (Table 1). The stress-strain behavior resembled the cryogels, displaying the typical three regions observed in polymeric materials without structural breakage, indicating a compact and stable structure. However, notable differences were observed compared to the corresponding cryogels. The hardness of oleogels was proportional to the biopolymer concentration, with S100C0 showing the highest value (15.3 N) due to the combination of density and oil-filled pores reinforcing the structure (Moradabbasi et al., 2022). Increasing starch content improved the oleogel's elastic modulus, while higher cellulose levels enhanced plasticity. This aligns with Gravelle et al. (2017), reported increased plasticity in stearyl alcohol-stearic acid oleogels with added ethylcellulose, and other studies linking oleogel elasticity to hardness (Tanti et al., 2016; Wang et al., 2023). Notably, oleogels were significantly harder than their corresponding cryogels, indicating oil's role in strengthening the polymer network. Similar hardness trends were observed by Thakur et al. (2022) for soybean oleogels (>20 Pa) and Zhao et al. (2020) who reported a maximum of ~6.5 Pa.

3.4.2. Rheological characterization in steady and oscillatory shear (SAOS)

The oleogel microstructure images were examined as they provide important insights into the microstructure arrangement in these complex fluids, specifically particle orientation and its consequence in the

flow anisotropy. The micrographs of the oleogels are depicted in Fig. 5 and correspond to their equilibrium conditions (i.e., the initial state of the microstructure) in the absence of shearing flows. The oleogel S100C0 (Fig. 5a) forms a type of reticulate due to the arrangement of the macromolecules of potato starch. In the micrograph of S50C50 (Fig. 5b), cotton cellulose fibers are dispersed in this reticulate of starch, whereas in the oleogel S0C100 (Fig. 5c) the presence of cellulose dominates the material structure. All initial particle configurations within the oleogels do not follow the most common statistically homogeneous distribution at the equilibrium condition of a fluid. Indeed, both the presence of reticulates of starch and fibers of cellulose makes the suspensions strongly anisotropic and consequently, the viscosity in the vicinity of equilibrium η_0 (i.e. as $\dot{\gamma} \to 0$) could not be evaluated in steady shear experiments. In other words, the apparent viscosity does not appear saturated as $\dot{\gamma}$ goes to zero.

The steady shear experiments (Fig. 6a) have shown that all oleogels tested presented a shear rate-dependent viscosity and behaved as pseudoplastic non-Newtonian fluids (i.e., shear thinning behavior). Their apparent viscosity decreased as the applied shear rate was enhanced. This behavior arises from the flow's interaction with the complex fluid's microstructure. As the shear rate increases, the flow acts more strongly on the potato starch and the anisotropic cellulose fibers. It first aligned these structures with the shear flow streamlines, reducing the collisional area of the structures undergoing shear. Consequently, this mechanism results in a smaller local dissipation within the fluid, which, in bulk terms, reflects the decrease in the viscosity observed. Another observation was that as the shear rate increases, another mechanism of structure breakup by the shearing flow might appear. In the oleogel scenario, the flow-induced structure breakup may probably be related to the reticulation of potato starch due to the high mechanical resistance of the cellulose fibers, which are degraded by the flow. All curves in Fig. 6a are fitted according to Sisko's model, given by: $\eta = \eta_\infty + k\dot{\gamma}^{n-1}$ as proposed in a different context by Pereira and Cunha (2020). The fitting parameters for each dataset are displayed at Table S2 (Supplementary Material). Alavi and Ciftci (2023) have also observed experimentally that oleogels composed of soybean presented a pseudo-plastic behavior described by a power-law model.

The behavior of the saturated viscosity value in the limit of higher shear rate, η_∞ (i.e., for strong flows) for the oleogels as a function of the mass fraction of cotton cellulose (w_c) is shown in Fig. 6b. Adding cellulose fibers substantially increased the fluid's viscosity from values less than 1 Pa·s to a value about six times greater (i.e., 6 Pa·s). This increase in the viscosity may occur even in a strong flow condition where the mechanism of intensively aligning and breaking microstructure probably dominates. This happens because the addition of cellulose fraction in the fluid increased the microstructure's complexity, making it very difficult for the flow to change shape, resulting in a more prominent local energy dissipation. The particle stress called stresslet (Batchelor, 1970a) is directly proportional to the structure volume or L^3, where L is the average size of the structure for a given shear rate. In addition, an
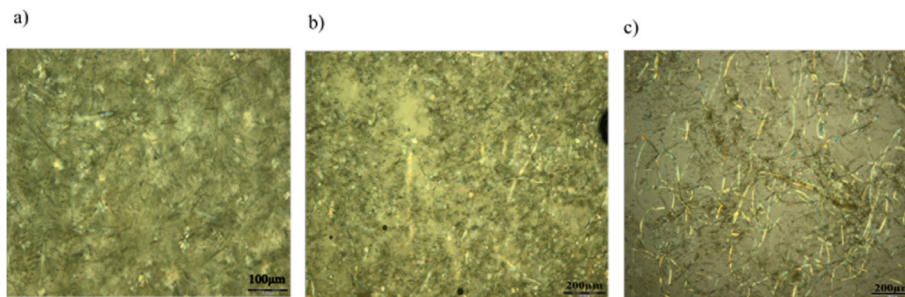
Fig. 5. Typical photomicrographs of a sample of the oleogels: (a) S100C0, (b) S50C50 and (c) S0C100 with 50× magnification.
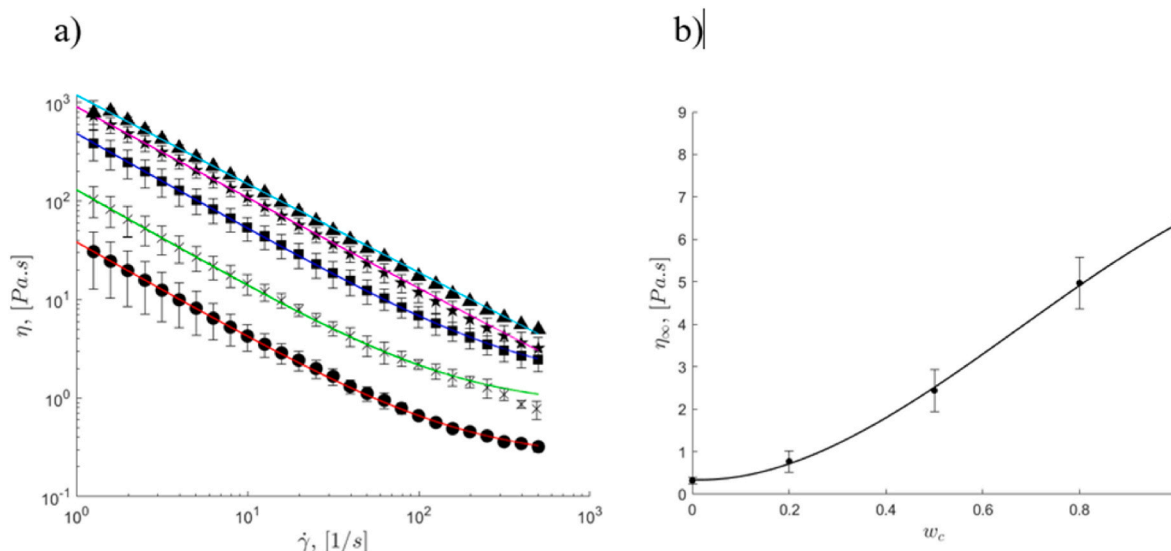

Fig. 6. (a) Apparent viscosity as a function of the shear-rate for the oleogels analyzed: ▲S0C100, ★ S20C80, ■ S50C50, × S80C20 and ● S100C0. Full-line corresponds to Sisko's model: $\eta = \eta_\infty + k\dot\gamma^{n-1}$ with fitting parameters for oleogels. (b) Effective viscosity as a function of the mass fraction of cellulose fiber. Full-line corresponds to the experimental data fitting with a third-order virial expansion: $\eta_\infty = b_0\left(1 + b_1 w_c + b_2 w_c^2 + b_3 w_c^3\right)$. *Here*, $b_0 = 0.34$, $b_1 = -1.22$, $b_3 = 37.09$ and $b_4 = -18.26$.

important finding is the viscosity's nonlinear dependence on the cellulose mass fraction. This finding indicates the presence of complex mechanisms internal to the fluid involving structures of different sizes interacting hydrodynamically (e.g., by the far-field viscous hydrodynamic interactions) and by near-field interactions like structure-collisions. Alavi and Ciftci (2023) have also observed experimentally that oleogels composed of soybean presented a pseudoplastic behavior described by a power-law model.

The tests in dynamic small amplitude oscillatory shear are very important to characterize the viscoelastic behavior of a complex fluid (Cwalina & Wagner, 2016; Völp & Willenbacher, 2021). It permits splitting into two different contributions: the elastic and viscous responses arising from the stress acting on the fluid. In this context, Fig. 7a shows the elastic modulus of the oleogels as a function of the forcing frequency.

As interest is to explore the behavior of the fluid near the equilibrium, as the fluid presents an anisotropic and coherent microstructure, the elastic modulus of all oleogels for the frequency ranging from 0 to 100 rad/s is invariant with ω. This is a typical behavior of a viscoelastic fluid which presents a solid-like behavior at low frequency. Under this condition, the shear elastic modulus, defined as $G_0 = \lim_{\omega \to 0} G'(\omega)$ and associated with a solid-like response, is evaluated for different values of the mass fraction of cotton cellulose fibers (w_c). The function $G_0(w_c)$ is the best quantity to characterize the elastic response of a viscoelastic fluid (Oliveira & Cunha, 2015; Völp & Willenbacher, 2021). As also demonstrated in Fig. 7a, an increase in the mass fraction of cellulose

fibers enhanced the G' at a given frequency and, as expected, G_0 increased with w_c as well (Fig. 7b). This behavior occurred because an increase in w_c implied a drastic change in the shape and distributions of structures within an oleogel, which resulted in strong correlations and interactions between neighboring structures and fiber-like agglomerates. This may substantially increment the resistance to shear an olegel from rest. Yield stress (σ_0) required for an oleogel to flow from an equilibrium state can be predicted as being $\sigma_0 = \gamma_0 G_0$. An interesting finding of this work is presented in Fig. 7b, demonstrating a strong dependence of G_0 on the mass fraction of cotton cellulose fibers, typically exponential. Alavi and Ciftci (2023) SAOS experiments were also carried out with frequencies ranging from 0.1 to 10 Hz for a fixed strain of 0.01 for a different oleogel-based soybean oil. However, the same authors present only a more superficial rheological analysis without determining or discussing from a physical point of view the origin and behavior of relevant rheological quantities of viscoelastic oleogels such as the shear elastic modulus and even the dynamic viscosity at very low-frequency response.

The dissipative (viscous) behavior of the oleogels was also examined using SAOS experiments (Cwalina & Wagner, 2016; Völp & Willenbacher, 2021). For this task, the loss modulus was plotted as a function of the forcing frequency (Fig. 7c). An increase in the mass fraction of cotton cellulose leads to an overall enhancement of the dissipative response of the fluid. As stated before, an increase in w_c may produce more complex structures of fiber agglomeration of larger sizes and, consequently, a larger particle stresslet, which varies with the
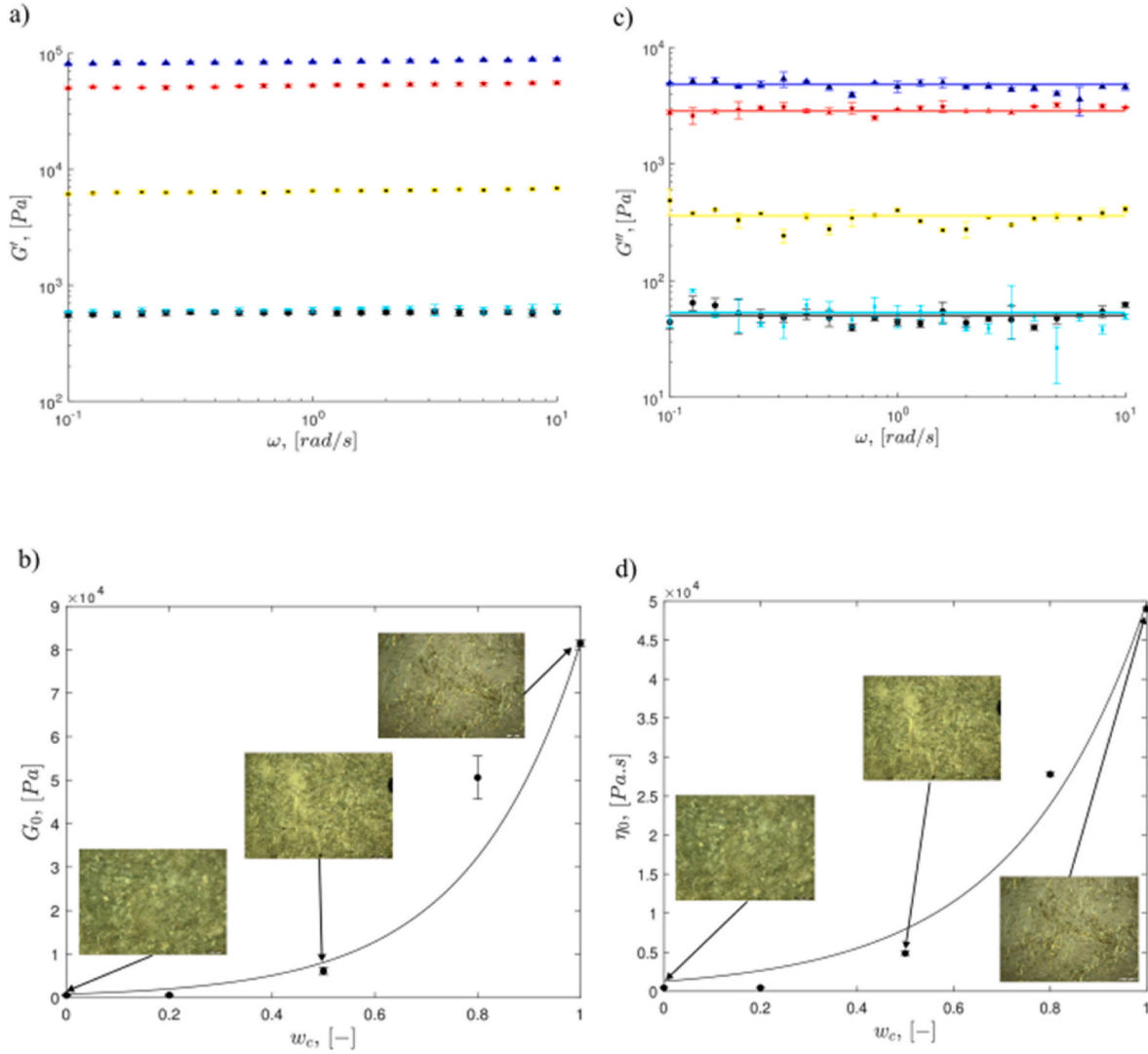
Fig. 7. (a) Storage modulus (elastic) G′, *(b)* Shear elastic modulus G_0, **(c)** Loss modulus (dissipation) G″ as a function of the forcing frequency ω **(d)** Viscosity in the vicinities of equilibrium η_0 as a function of the mass fraction of cotton cellulose fibers w_c for all examined oleogels: ▲ S0C100, ★ S20C80, ■ S50C50, × S80C20 *and* ● S100C0. The full line in (b) and (d) are exponential fits of the experimental datae: $\eta_0 = b_1\ exp(b_2 w_c)$, with $b_1 = 805$ and $b_2 = 46.2$ in (b) and $b_1 = 569$ and $b_2 = 45$ in (d). The associated error bars based on statistics over five experimental realizations are also shown in the plot for each experimental data.

average structure size L^3 (Batchelor, 1970b; Shaqfeh & Fredrickson, 1990). In addition, these larger fiber structures must interact with each other with a larger collisional area, resulting in a greater dissipation rate in the bulk flow. Furthermore, Fig. 7c shows a considerable increase in the value of the modulus G″ as w_c is incremented for the full range of frequency investigated in this study. Besides, the dissipative modulus persists nearly constant with the forcing frequency. Additionally, comparing the values of $G'(\omega)$ and $G''(\omega)$ it is seen values of G′ at least an order of magnitude higher than G″ for the full range of frequency explored. This shows that the oleogels behaved much more like an elastic solid at a low frequency than a viscous liquid, the same behavior observed by Sivakanthan et al. (2024) for stearic acid oleo gelated with beeswax. Papadaki et al. (2019) produced a soybean oleogel with G′ higher than G″ in the same order of magnitude.

Finally, from $G''(\omega)$ data, the effective zero-shear viscosity is extracted since $\eta_0 = \lim_{\omega\longrightarrow 0}\eta'(\omega)$, where $\eta'(\omega)$ is the so-called viscous modulus, defined as $\eta'(\omega) = G''/\omega$. The quantity η_0 deals with the viscous characteristics of the oleogels near to the equilibrium. As a result, applications in which the fluid remains for large periods of time at rest may use this important viscoelastic modulus to evaluate dissipative properties such as the fluid viscosity as a function of the mass fraction of ad-

ditives in oleogels like the cotton cellulose fibers. In contrast, with the algebraic dependence O(w_c^3) of η_∞ in strong flow (plotted in Fig. 6b), these results have suggested an exponential dependence of η_0 on w_c as shown in Fig. 7d, which was similar to the behavior of G_0 with w_c (Fig. 7b). To the better of our knowledge, there is no work reporting η_0 dependece with oleogel composition.

This contrast observed in viscosity behavior at low shear rates (weak flow condition) and viscosity at a high shear rates (strong flow) may be intrinsically related to the microstructural changes of the levels from equilibrium to strong flow conditions. It is expected that the interactions between the elements, such as fiber-aggregates of non-uniform and anisotropic shapes, in a small shear condition are much more complex than those in a condition of high shear rate. In particular, strong flows usually produce breakups and orientations of structures, resulting in a distribution of smaller structures oriented in the flow direction. In contrast, when the flow is weak, the structures persist large, with a large collisional area between the interactions of the fiber agglomerations dispersed in the ambient extract. This leads to much higher values of effective viscosity since the extra particle stresslet contribution increases with L^3, where L is a typical large structure size, which tends to increase with the mass fraction of the cotton fibers in the oleogels. These different

behaviors of the effective viscosity in weak and strong flows, characterized by a jump from exponential to algebraic dependence of the viscosity on the fraction of the fiber-additives, may be considered a remarkable finding of this rheological characterization of oleogels.

4. Conclusion

In conclusion, this study demonstrated that cellulose- and starch-based cryogels could be effectively transformed into oleogels using a simple oil sorption process. The composite cryogels showed superior mechanical strength, thermal stability, and oil-holding capacity compared to pure biopolymer cryogels. Cellulose provided reinforcement, enhancing flexibility and plasticity, while starch concentration influenced the oleogels' mechanical properties. Rheological analysis confirmed shear-thinning behavior and strong anisotropic properties, with higher cellulose content improving viscous and elastic properties, particularly at low frequencies where solid-like behavior was prominent. The unique viscosity behavior under varying flow conditions suggests internal structural transitions related to fiber aggregate size, orientation, and breakup. These results underscore the potential of cellulose and starch cryogels for oil absorption applications, such as oil spill cleanup, and for use in the food and pharmaceutical industries, leveraging the GRAS status of the materials. Finally, it should be noted that one of the main advantages of the work that considers the methodologies developed lies in the ability to control the thermal and mechanical properties of oleogels depending on the application required.

CRediT authorship contribution statement

Laiane Carvalho: Methodology, Investigation, Formal analysis, Data curation. **Igor Dal Osto Pereira:** Writing – original draft, Visualization, Methodology, Data curation, Investigation. **Larissa Andreani:** Writing – original draft, Resources, Project administration, Funding acquisition. **Francisco Ricardo Cunha:** Writing – review & editing, Supervision, Resources, Project administration, Methodology, Formal analysis, Conceptualization. **Sandra M. Luz:** Writing – original draft, Resources. **Rafael Macedo Dias:** Writing – original draft, Supervision, Methodology, Investigation. **Alysson M.A. Silva:** Supervision, Resources. **Leonardo F. Valadares:** Writing – original draft, Supervision, Resources, Project administration. **Simone Monteiro:** Writing – review & editing, Project administration, Funding acquisition.

Funding

Declaration of competing interest

The authors declare that they have no known competing financial interests or personal relationships that could have appeared to influence the work reported in this paper.

Appendix A. Supplementary data

Supplementary data to this article can be found online at https://doi.org/10.1016/j.lwt.2025.117406.

Data availability

Data will be made available on request.

References

Abdollahi, M., Goli, S. A. H., & Soltanizadeh, N. (2019). Physicochemical properties of foam-templated oleogel based on gelatin and xanthan gum. *European Journal of Lipid Science and Technology, 122*(2), 1–9. https://doi.org/10.1002/ejlt.201900196

Abdullah, Zou, Y. C., Farooq, S., Walayat, N., Zhang, H., Faieta, M., Pittia, P., & Huang, Q. (2022). Bio-aerogels: Fabrication, properties and food applications. *Critical Reviews in Food Science and Nutrition, 63*(24), 6687–6709. https://doi.org/10.1080/10408398.2022.2037504

Ago, M., Ferrer, A., & Rojas, O. J. (2016). Starch-based biofoams reinforced with lignocellulose nanofibrils from residual palm empty fruit bunches: Water sorption and mechanical strength. *ACS Sustainable Chemistry & Engineering, 4*(10), 5546–5552. https://doi.org/10.1021/acssuschemeng.6b01279

Aguayo, M. G., Fernández Pérez, A., Reyes, G., Oviedo, C., Gacitúa, W., Gonzalez, R., & Uyarte, O. (2018). Isolation and characterization of cellulose nanocrystals from rejected fibers originated in the kraft pulping process. *Polymers, 10*(10). https://doi.org/10.3390/polym10101145

Ahmad, K., Din, Z. ud, Ullah, H., Ouyang, Q., Rani, S., Jan, I., Alam, M., Rahman, Z., Kamal, T., Ali, S., Khan, S. A., Shahwar, D., Gul, F., Ibrahim, M., & Nawaz, T. (2022). Preparation and characterization of bio-based nanocomposites packaging films reinforced with cellulose nanofibers from unripe banana peels. *Starch/Staerke, 74* (5–6), 1–10. https://doi.org/10.1002/star.202100283

Alavi, F., & Ciftci, O. N. (2023). Effect of starch type and chitosan supplementation on physicochemical properties, morphology, and oil structuring capacity of composite starch bioaerogels. *Food Hydrocolloids, 141*(November 2022), Article 108637. https://doi.org/10.1016/j.foodhyd.2023.108637

Arboleda, J. C., Hughes, M., Lucia, L. A., Laine, J., Ekman, K., & Rojas, O. J. (2013). Soy protein-nanocellulose composite aerogels. *Cellulose, 20*(5), 2417–2426. https://doi.org/10.1007/s10570-013-9993-4

Barroso, N. G., Martins, A. J., Júnior, F. D. O., Okuro, P. K., Pereira, R. C., Vicente, A. A., Pastrana, L. M., Cunha, R. L., & Cerqueira, M. A. (2024). β-carotene and resveratrol loaded glycerol monostearate-based oleogels: Physicochemical characterization at low gelation concentrations. *Food Research International, 197*, Article 115181. https://doi.org/10.1016/J.FOODRES.2024.115181

Batchelor, G. K. (1970a). Slender-body theory for particles of arbitrary cross-section in Stokes flow. *Journal of Fluid Mechanics, 44*(3), 419–440. https://doi.org/10.1017/S002211207000191X

Batchelor, G. K. (1970b). The stress system in a suspension of force-free particles. *Journal of Fluid Mechanics, 41*(3), 545–570. https://doi.org/10.1017/S0022112070000745

Baudron, V., Gurikov, P., Smirnova, I., & Whitehouse, S. (2019). Porous starch materials via supercritical-and freeze-drying. *Gels, 5*(1), 9–13. https://doi.org/10.3390/gels5010012

Bird, R. B., Stewart, R. C., & Hassager, O. (1987). *Dynamic of polimeric liquids.* John Wiley & Son.

Chen, W., Abe, K., Uetani, K., Yu, H., Liu, Y., & Yano, H. (2014). Individual cotton cellulose nanofibers: Pretreatment and fibrillation technique. *Cellulose, 21*(3), 1517–1528. https://doi.org/10.1007/s10570-014-0172-z

Chen, W., Yu, H., Li, Q., Liu, Y., & Li, J. (2011). Ultralight and highly flexible aerogels with long cellulose i nanofibers. *Soft Matter, 7*(21), 10360–10368. https://doi.org/10.1039/c1sm06179h

Chen, K., & Zhang, H. (2020). Fabrication of oleogels via a facile method by oil absorption in the aerogel templates of protein-polysaccharide conjugates. *ACS Applied Materials and Interfaces, 12*(6), 7795–7804. https://doi.org/10.1021/acsami.9b21435

Cheng, H., Gu, B., Pennefather, M. P., Nguyen, T. X., Phan-Thien, N., & Duong, H. M. (2017). Cotton aerogels and cotton-cellulose aerogels from environmental waste for oil spillage cleanup. *Materials and Design, 130*(May), 452–458.

Ciftci, D., Ubeyitogullari, A., Huerta, R. R., Ciftci, O. N., Flores, R. A., & Saldaña, M. D. A. (2017). Lupin hull cellulose nanofiber aerogel preparation by supercritical CO2 and freeze drying. *The Journal of Supercritical Fluids, 127*(December 2016), 137–145.

Cwalina, C. D., & Wagner, N. J. (2016). Rheology of non-Brownian particles suspended in concentrated colloidal dispersions at low particle Reynolds number. *Journal of Rheology, 60*(1), 47–59. https://doi.org/10.1122/1.4935445

Davidovich-Pinhas, M. (2019). Oil structuring using polysaccharides. *Current Opinion in Food Science, 27*, 29–35.

Dogenski, M., Navarro-Díaz, H. J., de Oliveira, J. V., & Ferreira, S. R. S. (2020). Properties of starch-based aerogels incorporated with agar or microcrystalline cellulose. *Food Hydrocolloids, 108*(June), Article 106033.

Druel, L., Bardl, R., Vorwerg, W., & Budtova, T. (2017). Starch aerogels: A member of the family of thermal superinsulating materials. *Biomacromolecules, 18*(12), 4232–4239. https://doi.org/10.1021/acs.biomac.7b01272

Ek, P., Gu, B.-J., Saunders, S. R., Huber, K., & Ganjyal, G. M. (2021). Exploration of physicochemical properties and molecular interactions between cellulose and high-amylose cornstarch during extrusion processing. *Current Research in Food Science, 4*, 588–597. https://doi.org/10.1016/j.crfs.2021.07.001

Ghahremani, Y., Milani, J. M., Motamedzadegan, A., & Farmani, J. (2024). Fabrication of stable oleogel-in-water nanoemulsions with ethyl cellulose nanoparticles. *Lebensmittel-Wissenschaft & Technologie, 211*, Article 116900. https://doi.org/10.1016/j.lwt.2024.116900

Gill, S. K., Rossi, M., Bajka, B., & Whelan, K. (2021). Dietary fibre in gastrointestinal health and disease. *Nature Reviews Gastroenterology & Hepatology, 18*(2), 101–116. https://doi.org/10.1038/s41575-020-00375-4

Glasser, W. G., Atalla, R. H., Blackwell, J., Brown, M. M., Burchard, W., French, A. D., Klemm, D. O., & Nishiyama, Y. (2012). About the structure of cellulose: Debating the Lindman hypothesis. *Cellulose, 19*(3), 589–598. https://doi.org/10.1007/s10570-012-9691-7

Gravelle, A. J., Davidovich-Pinhas, M., Barbut, S., & Marangoni, A. G. (2017). Influencing the crystallization behavior of binary mixtures of stearyl alcohol and stearic acid (SOSA) using ethylcellulose. *Food Research International, 91*, 1–10. https://doi.org/10.1016/j.foodres.2016.11.024

Gu, H., Huo, X., Chen, J., El-Bahy, S. M., & El-Bahy Z, M. (2022). An overview of cellulose aerogel: Classification and applications. *ES Food & Agroforestry*, 1–9. https://doi.org/10.30919/esfaf782

Hassan, M. M., Tucker, N., & Le Guen, M. J. (2020). Thermal, mechanical and viscoelastic properties of citric acid-crosslinked starch/cellulose composite foams. *Carbohydrate Polymers, 230*(November 2019), Article 115675. https://doi.org/10.1016/j.carbpol.2019.115675

He, X., Chen, T., Jiang, T., Wang, C., Luan, Y., Liu, P., & Liu, Z. (2021). Preparation and adsorption properties of magnetic hydrophobic cellulose aerogels based on refined fibers. *Carbohydrate Polymers, 260*, Article 117790. https://doi.org/10.1016/j.carbpol.2021.117790

Jiang, Q., Li, P., Ji, M., Du, L., Li, S., Liu, Y., & Meng, Z. (2022). Synergetic effects of water-soluble polysaccharides for intensifying performances of oleogels fabricated by oil-absorbing cryogels. *Food Chemistry, 372*(September 2021), Article 131357. https://doi.org/10.1016/j.foodchem.2021.131357

Kavya, M., Udayarajan, C., Fabra, M. J., López-Rubio, A., & Nisha, P. (2022). Edible oleogels based on high molecular weight oleogelators and its prospects in food applications. *Critical Reviews in Food Science and Nutrition, 0*(0), 1–24. https://doi.org/10.1080/10408398.2022.2142195

Kenar, J. A., Eller, F. J., Felker, F. C., Jackson, M. A., & Fanta, G. F. (2014). Starch aerogel beads obtained from inclusion complexes prepared from high amylose starch and sodium palmitate. *Green Chemistry, 16*(4), 1921–1930. https://doi.org/10.1039/c3gc41895b

Lavoine, N., & Bergström, L. (2017). Nanocellulose-based foams and aerogels: Processing, properties, and applications. *Journal of Materials Chemistry A, 5*(31), 16105–16117. https://doi.org/10.1039/c7ta02807e

Lavoine, N., Desloges, I., Dufresne, A., & Bras, J. (2012). Microfibrillated cellulose - its barrier properties and applications in cellulosic materials: A review. *Carbohydrate Polymers, 90*(2), 735–764. https://doi.org/10.1016/j.carbpol.2012.05.026

Li, J., & Zhang, H. (2023). Efficient fabrication, characterization, and in vitro digestion of aerogel-templated oleogels from a facile method: Electrospun short fibers. *Food Hydrocolloids, 135*, Article 108185. https://doi.org/10.1016/j.foodhyd.2022.108185

Li, J., Zhang, C., Li, Y., & Zhang, H. (2022). Fabrication of aerogel-templated oleogels from alginate-gelatin conjugates for in vitro digestion. *Carbohydrate Polymers, 291* (December 2021). https://doi.org/10.1016/j.carbpol.2022.119603

Li, J., Zhao, S., Zhu, Q., & Zhang, H. (2023). Characterization of chitosan-gelatin cryogel templates developed by chemical crosslinking and oxidation resistance of camellia oil cryogel-templated oleogels. *Carbohydrate Polymers, 315*(May), Article 120971. https://doi.org/10.1016/j.carbpol.2023.120971

Liu, B., Sun, L., Jin, F., Wan, Y., Han, X., Fu, T., Guan, Y., Xie, Z., Cheng, L., Tian, B., & Feng, Z. (2023). A novel oleogel based on porous microgel from egg white. *Food Hydrocolloids, 144*(March), Article 109049. https://doi.org/10.1016/j.foodhyd.2023.109049

Manzocco, L., Valoppi, F., Calligaris, S., Andreatta, F., Spilimbergo, S., & Nicoli, M. C. (2017). Exploitation of κ-carrageenan aerogels as template for edible oleogel preparation. *Food Hydrocolloids, 71*, 68–75. https://doi.org/10.1016/j.foodhyd.2017.04.021

Mehling, T., Smirnova, I., Guenther, U., & Neubert, R. H. H. (2009). Polysaccharide-based aerogels as drug carriers. *Journal of Non-crystalline Solids, 355*(50–51), 2472–2479. https://doi.org/10.1016/j.jnoncrysol.2009.08.038

Moradabbasi, M., Goli, S. A. H., & Fayaz, G. (2022). Effect of biopolymers concentration and drying methods on physicochemical properties of emulsion-templated oleogel. *Journal of Food Science and Technology, 59*(5), 1994–2003. https://doi.org/10.1007/s13197-021-05214-1

Nordin, N., Othman, S. H., Kadir Basha, R., & Abdul Rashid, S. (2018). Mechanical and thermal properties of starch films reinforced with microcellulose fibres. *Food Research, 2*(6), 555–563. https://doi.org/10.26656/fr.2017.2(6).110

Oliveira, T. F., & Cunha, F. R. (2015). Emulsion rheology for steady and oscillatory shear flows at moderate and high viscosity ratio. *Rheologica Acta, 54*(11–12), 951–971. https://doi.org/10.1007/S00397-015-0885-4

Ong, K. J., Ede, J. D., Pomeroy-Carter, C. A., Sayes, C. M., Mulenos, M. R., & Shatkin, J. A. (2020). A 90-day dietary study with fibrillated cellulose in Sprague-Dawley rats. *Toxicology Reports, 7*(January), 174–182. https://doi.org/10.1016/j.toxrep.2020.01.003

Pääkkö, M., Vapaavuori, J., Silvennoinen, R., Kosonen, H., Ankerfors, M., Lindström, T., Berglund, L. A., & Ikkala, O. (2008). Long and entangled native cellulose i nanofibers allow flexible aerogels and hierarchically porous templates for functionalities. *Soft Matter, 4*(12), 2492–2499. https://doi.org/10.1039/b810371b

Papadaki, A., Kopsahelis, N., Mallouchos, A., Mandala, I., & Koutinas, A. A. (2019). Bioprocess development for the production of novel oleogels from soybean and microbial oils. *Food Research International, 126*, Article 108684. https://doi.org/10.1016/j.foodres.2019.108684

Park, S., Baker, J. O., Himmel, M. E., Parilla, P. A., & Johnson, D. K. (2010). Cellulose crystallinity index: Measurement techniques and their impact on interpreting

cellulase performance. *Biotechnology for Biofuels, 3*(1), 10. https://doi.org/10.1186/1754-6834-3-10

Patel, A. R. (2018). In *Crystallization of lipids: Fundamentals and applications in food, cosmetics, and pharmaceuticals* (1st ed.). John Wiley & Sons Ltd. Wiley. https://doi.org/10.1002/9781118593882.ch13

Patel, A. R., Rajarethinem, P. S., Cludts, N., Lewille, B., De Vos, W. H., Lesaffer, A., & Dewettinck, K. (2015). Biopolymer-based structuring of liquid oil into soft solids and oleogels using water-continuous emulsions as templates. *Langmuir, 31*(7), 2065–2073. https://doi.org/10.1021/la502829u

Patel, A. R., Schatteman, D., Lesaffer, A., & Dewettinck, K. (2013). A foam-templated approach for fabricating organogels using a water-soluble polymer. *RSC Advances, 3* (45), 22900–22903. https://doi.org/10.1039/c3ra44763d

Paulauskiene, T., Teresiute, A., Uebe, J., & Tadzijevas, A. (2022). Sustainable cross-linkers for the synthesis of cellulose-based aerogels: Research and application. *Journal of Marine Science and Engineering, 10*(4). https://doi.org/10.3390/jmse10040491

Pereira, I. D. O., & Cunha, F. R. (2020). Rheological response in shear flows of a thermosensitive elastic liquid in the presence of some additives. *Rheologica Acta, 59* (5), 307–316. https://doi.org/10.1007/S00397-020-01194-9/FIGURES/8

Pereira, I. D. O., & Cunha, F. R. (2023). Rheological response of ferrofluids undergoing unsteady shear flows in the presence of a magnetic field. *Physics of Fluids, 35*(11), Article 112008. https://doi.org/10.1063/5.0171084

Poletto, M., Ornaghi Júnior, H. L., & Zattera, A. J. (2014). Native cellulose: Structure, characterization and thermal properties. *Materials, 7*(9), 6105–6119. https://doi.org/10.3390/ma7096105

Puscas, A., Muresan, V., Socaciu, C., & Muste, S. (2020). Oleogels in food: A review of current and potential applications. *Foods, 9*(1), 1–27. https://doi.org/10.3390/foods9010070

Ratnayake, W. S., & Jackson, D. S. (2007). A new insight into the gelatinization process of native starches. *Carbohydrate Polymers, 67*(4), 511–529. https://doi.org/10.1016/j.carbpol.2006.06.025

Rongpipi, S., Ye, D., Gomez, E. D., & Gomez, E. W. (2019). Progress and opportunities in the characterization of cellulose – an important regulator of cell wall growth and mechanics. *Frontiers in Plant Science, 9*(March), 1–28. https://doi.org/10.3389/fpls.2018.01894

Sehaqui, H., Salajková, M., Zhou, Q., & Berglund, L. A. (2010). Mechanical performance tailoring of tough ultra-high porosity foams prepared from cellulose i nanofiber suspensions. *Soft Matter, 6*(8), 1824–1832. https://doi.org/10.1039/b927505c

Sehaqui, H., Zhou, Q., & Berglund, L. A. (2011). High-porosity aerogels of high specific surface area prepared from nanofibrillated cellulose (NFC). *Composites Science and Technology, 71*(13), 1593–1599. https://doi.org/10.1016/j.compscitech.2011.07.003

Shaqfeh, E. S. G., & Fredrickson, G. H. (1990). The hydrodynamic stress in a suspension of rods. *Physics of Fluids A: Fluid Dynamics, 2*(1), 7–24. https://doi.org/10.1063/1.857683

Siqueira, G., Bras, J., & Dufresne, A. (2010). Cellulosic bionanocomposites: A review of preparation, properties and applications. *Polymers, 2*(4), 728–765. https://doi.org/10.3390/polym2040728

Spiridon, I., Teacă, C. A., Bodîrlău, R., & Bercea, M. (2013). Behavior of cellulose reinforced cross-linked starch composite films made with tartaric acid modified starch microparticles. *Journal of Polymers and the Environment, 21*(2), 431–440. https://doi.org/10.1007/s10924-012-0498-2

Tanti, R., Barbut, S., & Marangoni, A. G. (2016). Hydroxypropyl methylcellulose and methylcellulose structured oil as a replacement for shortening in sandwich cookie creams. *Food Hydrocolloids, 61*, 329–337.

Teles dos Santos, M., Gerbaud, V., & Roux, G. A. C. Le (2013). Modeling and simulation of melting curves and chemical interesterification of binary blends of vegetable oils. *Chemical Engineering Science, 87*, 14–22. https://doi.org/10.1016/j.ces.2012.09.026

Teles, V. C., Roldi, M., Luz, S. M., Santos, W. R., Andreani, L., & Valadares, L. F. (2021). Obtaining plasticized starch and microfibrillated cellulose from oil palm empty fruit bunches: Preparation and properties of the pure materials and their composites. *Bioresources*, 3746–3759.

Thakur, D., Singh, A., Prabhakar, P. K., Meghwal, M., & Upadhyay, A. (2022). Optimization and characterization of soybean oil-carnauba wax oleogel. *Lebensmittel-Wissenschaft & Technologie, 157*, Article 113108. https://doi.org/10.1016/j.lwt.2022.113108

Völp, A. R., & Willenbacher, N. (2021). Shear modulus and yield stress of foams: Contribution of interfacial elasticity. *Soft Matter, 17*(14), 3937–3944. https://doi.org/10.1039/D0SM02246B

Wüstenberg, T. (2014). General overview of food hydrocolloids. In T. Wüstenberg (Ed.), *Cellulose and cellulose derivatives in the food industry* (1st ed., pp. 1–68). https://doi.org/10.1002/9783527682935.ch01

Wang, J., Chen, Z., & Naguib, H. E. (2021). Preparation of a novel double crosslinked chitin aerogel via etherification with high strength. *Carbohydrate Polymers, 265* (November 2020), Article 118014. https://doi.org/10.1016/j.carbpol.2021.118014

Wang, Q., Espert, M., Larrea, V., Quiles, A., Salvador, A., & Sanz, T. (2023). Comparison of different indirect approaches to design edible oleogels based on cellulose ethers. *Food Hydrocolloids, 134*(June 2022), Article 108007. https://doi.org/10.1016/j.foodhyd.2022.108007

Wang, S., Li, C., Copeland, L., Niu, Q., & Wang, S. (2015). Starch retrogradation: A comprehensive review. *Comprehensive Reviews in Food Science and Food Safety, 14*(5), 568–585. https://doi.org/10.1111/1541-4337.12143

Wang, S., Peng, X., Zhong, L., Tan, J., Jing, S., Cao, X., Chen, W., Liu, C., & Sun, R. (2015). An ultralight, elastic, cost-effective, and highly recyclable superabsorbent from microfibrillated cellulose fibers for oil spillage cleanup. *Journal of Materials Chemistry A, 3*(16), 8772–8781. https://doi.org/10.1039/C4TA07057G

Wang, C., Wang, X., Liu, C., & Liu, C. (2021). Application of LF-NMR to the characterization of camellia oil-loaded pickering emulsion fabricated by soy protein isolate. *Food Hydrocolloids, 112*(April 2020), Article 106329. https://doi.org/10.1016/j.foodhyd.2020.106329

Wang, Y., Wu, K., Xiao, M., Riffat, S. B., Su, Y., & Jiang, F. (2018). Thermal conductivity, structure and mechanical properties of konjac glucomannan/starch based aerogel strengthened by wheat straw. *Carbohydrate Polymers, 197*, 284–291. https://doi.org/10.1016/j.carbpol.2018.06.009

Yang, S., Yang, G., Chen, X., Chen, J., & Liu, W. (2020). Interaction of monopalmitate and carnauba wax on the properties and crystallization behavior of soybean oleogel. *Grain & Oil Science and Technology, 3*(2), 49–56. https://doi.org/10.1016/j.gaost.2020.05.001

Yang, S., Zhang, X., Saleh, A. S. M., Wang, L., Duan, Y., & Xiao, Z. (2024). Effect of β-sitosterol and palmitic acid mass ratio on structural, physicochemical, and rheological properties of rice bran oil-based oleogel. *Lebensmittel-Wissenschaft & Technologie, 209*, Article 116775. https://doi.org/10.1016/j.lwt.2024.116775

Yildirim, N., Shaler, S. M., Gardner, D. J., Rice, R., & Bousfield, D. W. (2014). Cellulose nanofibril (CNF) reinforced starch insulating foams. *Cellulose, 21*(6), 4337–4347. https://doi.org/10.1007/s10570-014-0450-9

Zhao, M., Lan, Y., Cui, L., Monono, E., Rao, J., & Chen, B. (2020). Physical properties and cookie-making performance of oleogels prepared with crude and refined soybean oil: A comparative study. *Food & Function, 11*(3), 2498–2508. https://doi.org/10.1039/C9FO02180A

Zhao, Y. W., Tian, M. Z., & Huang, P. (2021). Starch/clay aerogel reinforced by cellulose nanofibrils for thermal insulation. *Cellulose, 28*(6), 3505–3513. https://doi.org/10.1007/s10570-021-03750-9

Zhao, W., Wei, Z., Xue, C., & Meng, Y. (2023). Development of food-grade oleogel via the aerogel-templated method: Oxidation stability, astaxanthin delivery and emulsifying application. *Food Hydrocolloids, 134*, Article 108058. https://doi.org/10.1016/j.foodhyd.2022.108058

Zhu, F. (2019). Starch based aerogels: Production, properties and applications. *Trends in Food Science and Technology, 89*(March), 1–10. https://doi.org/10.1016/j.tifs.2019.05.001

Zou, F., & Budtova, T. (2020). Tailoring the morphology and properties of starch aerogels and cryogels via starch source and process parameter. *Carbohydrate Polymers, 255*(October), Article 117344. https://doi.org/10.1016/j.carbpol.2020.117344